PASJ: Publ. Astron. Soc. Japan **46**, 27–43 (1994)

Spectroscopic Study of the Be Star Phi Persei

Mahendra SINGH, * Masahiro MON, and Tomokazu KOGURE†
Department of Astronomy, Faculty of Science, Kyoto University, Sakyo-ku, Kyoto 606
E-mail(MM) mon@kusastro.kyoto-u.ac.jp
and
Masakazu SUZUKI
Kanazawa Institute of Technology, P.O. Kanazawa-South, Ishikawa 921

(Received 1992 November 2; accepted 1993 September 27)

Abstract

Based on a series of Coudé spectra taken with the 188-cm reflector of the Okayama Astrophysical Observatory over an interval of 18 yr, the spectroscopic behavior in the Balmer and He I λ3888 lines of the binary Be star ϕ Per (orbital period of 126.696 d) is presented. We have confirmed the following phenomena: (1) the V/R ratio (intensity ratio of violet to red peaks of the double-peaked emission lines) varies synchronously with the binary phase, and its amplitude is about 2; (2) the shell absorption lines become very strong at a phase of around 0.1; (3) there is a remarkable hump in the radial velocity curve of the shell lines near to phases of 0.4 to 0.6; and (4) the peak separations of the emission lines do not vary with the phase, but remain constant.

It seems difficult to represent the ϕ Per phenomena sited above with the simple envelope models which have so far been adopted for many Be stars. The difficulties are pointed out for the axisymmetric rotating-pulsating envelope model and the elliptic disk model with apsidal motion. The formation of a high-density region around the primary is required for the appearance of a strong shell at a particular phase. The hump in the radial-velocity curves requires that the envelope around the primary should be elongated perpendicular to the binary axis. Using the peak separations of the Balmer emission lines, a large extension of the envelope which overflows the Roche lobe of the primary was estimated. This infers that an envelope really extends beyond the Roche lobe and thus may be a very complicated one, or that the binary parameters so far adopted ($20\,M_\odot$ and $4\,M_\odot$) are not reliable. The possibility of less massive binary parameters is suggested.

Key words: Line profiles — Radial velocities — Stars: Be stars — Stars: binaries — Stars: individual (ϕ Per)

1. Introduction

ϕ Per is a well-known spectroscopic binary Be (shell) star with the spectral type B2 IVep (Lesh 1968) and a rapid rotation of $V \sin i = 450$ km s^{-1} (Poeckert 1981). Since early observations by Campbell (1902), this star has been extensively observed by Lockyer (1925, 1926), Hynek (1940, 1944), Hickok (1969), Hendry (1976), and others.

Suzuki (1980) has studied Hynek's (1940) radial velocity data of shell absorptions and of emission peaks by applying a restricted three-body problem. He concluded that the masses of the binary components are 20 $M_\odot$ for the primary and 4 $M_\odot$ for the secondary with a separation of 1.42 AU. On the other hand, Poeckert (1981) has carried out a series of high-dispersion and high signal-to-noise ratio spectroscopic observations, and estimated the masses of the binary components as being 21 $M_\odot$ for the primary and 3.4 $M_\odot$ for the secondary, based on an analysis of the radial velocity curves for both components.

Lockyer (1925, 1926) first noticed its V/R variability synchronized with the orbital phase and the existence of a strong shell feature in the Balmer series at a particular phase of 0.05 to 0.15, where the shell absorption feature is seen up to H23 or so. ϕ Per is generally a weak shell star, that is, the shell absorption lines that are visible throughout the binary phase are only the lower members of the Balmer series, lower than H7 or so, and the strong He I line at λ3888 ($2s^3S - 3p^3P^o$).

Poeckert (1981) has analysed the emission lines of the Balmer series, Fe II, and He II as well as the shell lines of the Balmer series and He I, and has given a picture in which the envelope is denser (or more extended) in the region facing the secondary. With this picture he explained the observed cyclic V/R variation and a strong

* Present address: Uttar Pradesh State Observatory, Manora Peak, Naini Tal, 263129, India.
† Present address: Bisei Astronomical Observatory, 1723-70, Ohkura, Bisei, Oda-gun, Okayame 714-14.

He I shell phase (between 0.4 and 0.6) which he has found.

Recently, Brown (1992) studied the photometric variation of this star, and reported that abrupt minima of about 0.1 mag exist in the V band at phases of around 0.1 and 0.5. These correspond to the strong shell phases of the hydrogen and helium lines, respectively.

In this paper we present our new spectroscopic data of ϕ Per obtained at the Okayama Astrophysical Observatory. Our observational data are based on photographic spectral plates and are not of sufficiently high signal-to-noise ratio compared to those of Poeckert (1981); we thus confined our study to some remarkable spectroscopic behaviors of the hydrogen and He I lines. We measured the radial velocities and line intensities at some characteristic points of the spectral line profiles.

Based on these measurements we consider the structure of the envelope around the primary star, with particular attention to its form and extension as well as its physical behavior in the strong shell phase. We re-examine the binary parameters, because the envelope structure appreciably depends on the mass of the central star.

The observational data are presented in the next section. The results are given in section 3. We first examine the radial velocities and discuss the binary model in section 4. The emission-line profiles are analysed in section 5 along with some discussion concerning the envelope structure. A strong shell phase is considered in section 6.

2. Observational Data and Measurements

Table 1 lists the 91 spectrograms of ϕ Per which were obtained between 1968 and 1986 with the Coudé spectrograph of the 188-cm reflector of the Okayama Astrophysical Observatory. All of the observational data were folded for the orbital period of 126.696 d with an epoch of T_0 = JD 2424473.500 (Hickok 1969) in order to see the phase dependence of the physical parameters. The plate number, date of observation, Julian day, emulsion, spectral region (in Angstrom), and orbital phase (Hickok 1969) are given in table 1.

The reciprocal dispersions are about 10 Å mm^{-1} and 20 Å mm^{-1} for the blue and red regions, respectively, for the plates labeled by C4, and about 4 Å mm^{-1} for the blue plates labeled by C10.

All of the plates were measured with the PDS (PE) microdensitometer at the Kwasan Observatory, Kyoto University. With the aid of software developed by one of the authors, data reductions were processed at the Computer Center of Kanazawa Institute of Technology and at the Data Processing Center of Kyoto University.

The radial velocities (RV) and line intensities were measured at some characteristic points of the profile, as illustrated in figure 1.

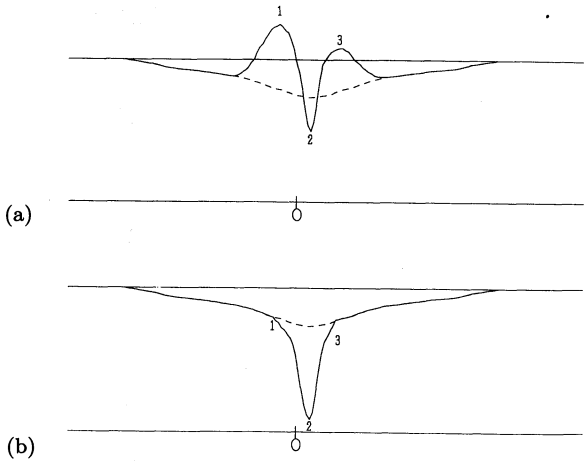

Fig. 1. Schematic diagram of the line profiles representing how the radial velocities and intensities at different points were measured. (a) Balmer line and (b) He I λ3888 shell line. The interpolated photospheric profiles are indicated by dashed lines and the mark O represents the laboratory wavelength of the line center.

In the case of the Balmer lines, the radial velocities and intensity values at three different points were measured (figure 1a). Points 1 and 3 give the emission peak velocities ($RV_{\rm eb}$, $RV_{\rm er}$) and intensities ($I_{\rm eb}$, $I_{\rm er}$). Point 2 gives the radial velocity ($RV_{\rm ac}$) and intensity ($I_{\rm ac}$) for the central absorption. The values of $I_{\rm eb}$ and $I_{\rm er}$ were measured as the excess heights from the interpolated photospheric line (dotted) and $I_{\rm ac}$ was measured from the zero level. In the case of the He I λ3888 shell line, the radial velocity for the central absorption at point 2 ($RV_{\rm ac}$) and the intensity values at points 1, 2, 3 ($I_{\rm ab}$, $I_{\rm ac}$, $I_{\rm ar}$) were measured (figure 1b). All of these intensities were measured from the zero level.

The radial velocities are corrected for the heliocentric values and the intensities were measured in units of the adjacent continuum. The central parts of the photospheric lines were determined beforehand by an interpolation of the profiles from the wing parts, while considering the spectral type and projected rotational velocity of ϕ Per.

3. Results

The results of the measurements are given in tables 2 (Balmer lines) and 3 (He I λ3888). The estimated error of the measurement for the radial velocity of the shell absorption is typically 5 km s^{-1} and that for the intensity is 10 percent. These estimations were made with the data obtaied from the plates observed on the same date (C4–4919 to C4–4925, cf. table 1). The plate number, phase

Table 1. List of spectrograms of ϕ Per.

	Plate number	Date	Julian day 2440000+	Emulsion	Spectral region (Ångstrom)	Period
1	C4 – 2154	1968 24 08	0093.19	103 a O	3700 – 4600	123.285
2	C4 – 2155	1968 24 08	0093.22	103 a O	3500 – 4300	123.285
3	C4 – 2156	1968 24 08	0093.23	103 a F	5500 – 7200	123.285
4	C4 – 2263	1968 05 12	0196.02	103 a O	4300 – 5100	124.096
5	C4 – 2264	1968 05 12	0196.03	103 a O	3850 – 4700	124.096
6	C4 – 2265	1968 05 12	0196.04	103 a O	3500 – 4300	124.097
7	C4 – 2266	1968 05 12	0196.05	103 a F	5500 – 7200	124.097
8	C4 – 2364	1969 28 08	0462.28	103 a O	3500 – 4300	126.198
9	C4 – 2379	1969 30 08	0464.25	103 a O	3700 – 4600	126.214
10	C4 – 2441	1969 22 12	0578.02	103 a F	5500 – 7200	127.112
11	C4 – 2442	1969 22 12	0578.04	103 a O	3500 – 4300	127.112
12	C4 – 2443	1969 22 12	0578.05	103 a O	3700 – 4600	127.112
13	C4 – 2444	1969 22 12	0578.06	103 a O	4300 – 5100	127.112
14	C4 – 2471	1969 24 12	0579.99	103 a F	5500 – 7200	127.127
15	C4 – 2472	1969 24 12	0580.00	103 a O	4300 – 5100	127.127
16	C4 – 2473	1969 24 12	0580.02	103 a O	3700 – 4600	127.127
17	C4 – 2474	1969 24 12	0580.03	103 a O	3500 – 4300	127.127
18	C4 – 2475	1969 24 12	0580.05	103 a F	5500 – 7200	127.128
19	C4 – 3102	1971 13 08	1177.24	II a O^+	3500 – 4300	131.841
20	C4 – 3103	1971 13 08	1177.25	II a F	5500 – 7200	131.841
21	C4 – 4533	1975 20 11	2736.07	103 a O	3500 – 4300	144.145
22	C4 – 4534	1975 20 11	2736.08	103 a O	3850 – 4700	144.145
23	C4 – 4535	1975 20 11	2736.08	103 a O	4300 – 5100	144.145
24	C4 – 4845	1976 09 11	3091.96	II a F	5300 – 6950	146.954
25	C4 – 4846	1976 09 11	3091.97	103 a O	3500 – 4300	146.954
26	C4 – 4847	1976 09 11	3091.98	103 a O	3500 – 4300	146.954
27	C4 – 4848	1976 09 11	3091.98	103 a O	4300 – 5100	146.954
28	C4 – 4919	1976 09 12	3121.89	103 a O	3700 – 4600	147.190
29	C4 – 4920	1976 09 12	3121.90	103 a O	3700 – 4600	147.190
30	C4 – 4921	1976 09 12	3121.91	103 a O	3700 – 4600	147.190
31	C4 – 4922	1976 09 12	3121.92	103 a O	3700 – 4600	147.190
32	C4 – 4923	1976 09 12	3121.94	103 a O	3700 – 4600	147.190
33	C4 – 4924	1976 09 12	3121.94	103 a O	3700 – 4600	147.190
34	C4 – 4925	1976 09 12	3121.95	103 a O	3700 – 4600	147.191
35	C4 – 4929	1976 10 12	3122.95	103 a O	3700 – 4600	147.198
36	C4 – 4934	1976 10 12	3122.97	103 a O	3700 – 4600	147.199
37	C4 – 4935	1976 10 12	3122.97	103 a O	3700 – 4600	147.199
38	C4 – 4936	1976 10 12	3122.98	103 a O	3700 – 4600	147.199
39	C10 – 3253	1976 11 12	3123.13	103 a O	3800 – 4300	147.200
40	C10 – 3254	1976 11 12	3123.13	103 a O	3800 – 4300	147.200
41	C10 – 3263	1976 12 12	3124.13	103 a O	3800 – 4300	147.208
42	C10 – 3264	1976 12 12	3124.13	103 a O	3800 – 4300	147.208
43	C4 – 5474	1978 15 11	3828.10	II a O^+	3500 – 4300	152.764
44	C4 – 5475	1978 15 11	3828.11	II a O^+	3850 – 4700	152.764
45	C4 – 5476	1978 15 11	3828.12	II a F	5300 – 6950	152.764
46	C4 – 5481	1978 16 11	3828.98	II a O^+	4300 – 5100	152.771
47	C4 – 5720	1979 29 11	4207.06	II a O^+	3500 – 4300	155.755
48	C4 – 5784	1980 25 01	4264.09	II a O^+	4200 – 5000	156.205
49	C4 – 5795	1980 27 01	4266.03	II a O^+	4200 – 5000	156.221
50	C4 – 5800	1980 27 01	4266.06	II a O^+	3600 – 4450	156.221

Table 1. (Continued).

	Plate number	Date	Julian day 2440000+	Emulsion	Spectral region (Ångstrom)	Period
51	C4 – 5882	1980 24 11	4567.99	II a O^+	3850 – 4700	158.604
52	C4 – 5883	1980 24 11	4568.01	II a O	3500 – 4300	158.604
53	C4 – 5884	1980 24 11	4568.04	II a O	4300 – 5100	158.604
54	C4 – 5885	1980 24 11	4568.10	II a F	5500 – 7200	158.605
55	C4 – 5886	1980 24 11	4568.10	II a O	3850 – 4700	158.605
56	C4 – 5887	1980 24 11	4568.12	II a O	3850 – 4700	158.605
57	C4 – 5927	1981 23 01	4627.89	II a O	3950 – 4800	159.077
58	C4 – 5928	1981 23 01	4627.90	II a O	3950 – 4800	159.077
59	C4 – 5932	1981 23 01	4627.92	II a O	3950 – 4800	159.077
60	C4 – 6196	1981 11 12	4950.06	II a O^+	4300 – 5100	161.620
61	C4 – 6207	1981 12 12	4951.05	II a O^+	3600 – 4450	161.627
62	C4 – 6208	1981 12 12	4951.09	II a O^+	4200 – 5000	161.628
63	C4 – 6223	1981 15 12	4953.99	II a O^+	4200 – 5000	161.651
64	C4 – 6224	1981 15 12	4954.00	II a O^+	3700 – 4600	161.651
65	C4 – 6232	1981 16 12	4955.10	II a O^+	3600 – 4450	161.659
66	C4 – 6233	1981 16 12	4955.11	II a O^+	4200 – 5000	161.659
67	C10 – 4050	1982 03 09	5215.31	103 a O	3900 – 4400	163.713
68	C4 – 6424	1982 01 12	5305.02	II a O	3500 – 4300	164.421
69	C4 – 6425	1982 01 12	5305.03	II a O	3500 – 4300	164.421
70	C4 – 6426	1982 01 12	5305.05	II a O	3500 – 4300	164.421
71	C4 – 6427	1982 01 12	5305.06	II a O	4300 – 5100	164.422
72	C4 – 6428	1982 01 12	5305.07	II a O	4300 – 5100	164.422
73	C4 – 6429	1982 01 12	5305.09	II a O	4300 – 5100	164.422
74	C4 – 6812	1983 21 10	5629.01	II a O^+	3600 – 4450	166.979
75	C4 – 6814	1983 21 10	5629.02	II a O^+	4200 – 5000	166.979
76	C4 – 6815	1983 21 10	5629.03	II a O^+	4200 – 5000	166.979
77	C4 – 6816	1983 21 10	5629.04	II a O^+	3600 – 4450	166.979
78	C4 – 6817	1983 21 10	5629.05	II a O^+	3600 – 4450	166.979
79	C4 – 6829	1983 22 10	5630.22	II a O^+	4200 – 5000	166.988
80	C4 – 6830	1983 22 10	5630.23	II a O^+	4200 – 5000	166.988
81	C4 – 6831	1983 22 10	5630.23	II a O	4200 – 5000	166.988
82	C4 – 6875	1983 23 12	5692.07	II a O^+	4200 – 5000	167.476
83	C4 – 6876	1983 23 12	5692.08	II a O^+	3600 – 4450	167.476
84	C4 – 6878	1983 23 12	5692.09	II a O^+	4300 – 5100	167.476
85	C4 – 6894	1983 24 12	5693.00	II a O^+	4300 – 5100	167.484
86	C4 – 6895	1983 24 12	5693.03	II a O^+	3600 – 4450	167.484
87	C4 – 7104	1985 26 10	6365.11	II a O^+	3500 – 4300	172.788
88	C4 – 7105	1985 26 10	6365.12	II a O^+	4100 – 4900	172.789
89	C4 – 7194	1986 22 10	6726.05	103 a F	5000 – 6700	175.637
90	C4 – 7195	1986 22 10	6726.10	II a O^+	3600 – 4450	175.638
91	C4 – 7196	1986 22 10	6726.11	II a O^+	4200 – 5000	175.638

$^+$ Represents baked emulsion

without referring to the period, and measured values at three points (figure 1a) are given in table 2 along with the logarithmic value of V/R in the last column. The results for Hβ are given in table 2-1, for Hγ in table 2-2, and for Hδ (without V/R values because of the poor accuracy) in table 2-3. In table 3, the plate number, phase, and measured values at three points (figure 1b) for the He I line are given along with the equivalent width (E.W.) and the full width at half intensity (F.W.) of the shell component. The full width at half intensity was measured for checking the blending with hydrogen H8 line.

Photospheric lines are generally so broad and shallow that the radial velocities for photospheric lines were not measured on our spectrograms. Poeckert (1981) has determined the radial-velocity curve for the photospheric

Table 2. Radial velocity data and intensities for the Balmer lines of ϕ Per.

Table 2-1 Hβ

	Plate No.	Phase	RV_{eb}	I_{eb}	RV_{ac}	I_{ac}	RV_{er}	I_{er}	$\log \frac{I_{eb}}{I_{er}}$
1	C4 – 2263	0.096	−110	0.72	10	1.04	90	0.66	0.04
2	C4 – 2444	0.112	−110	0.80	20	1.00	120	0.66	0.08
3	C4 – 2472	0.127	−95	0.79	10	1.00	115	0.70	0.05
4	C4 – 4535	0.145	−105	0.92	20	0.90	120	0.88	0.02
5	C4 – 5784	0.205	−75	1.01	17	1.00	105	0.60	0.23
6	C4 – 5795	0.221	−90	1.10	25	0.99	120	0.64	0.24
7	C4 – 6427	0.422	−105	0.90	−15	1.32	80	1.00	−0.05
8	C4 – 6428	0.422	−95	0.83	2	1.24	90	0.80	0.02
9	C4 – 6429	0.422	−95	0.80	−2	1.20	90	0.88	−0.04
10	C4 – 6878	0.476	−110	0.68	−10	1.20	90	1.00	−0.17
11	C4 – 6894	0.484	−110	0.66	−10	1.32	80	1.02	−0.19
12	C4 – 5884	0.604	−130	0.80	−5	1.26	80	1.22	−0.18
13	C4 – 6196	0.620	−110	0.60	−10	1.26	80	1.10	−0.26
14	C4 – 6208	0.628	−120	0.60	−15	1.30	70	1.10	−0.26
15	C4 – 6223	0.651	−120	0.62	−25	1.30	60	1.16	−0.28
16	C4 – 6233	0.659	−125	0.72	−15	1.24	60	1.40	−0.29
17	C4 – 5481	0.771	−125	0.62	−20	1.22	75	0.92	−0.17
18	C4 – 4848	0.954	−85	0.86	5	1.30	110	0.82	0.02
19	C4 – 6814	0.979	−110	0.66	10	1.28	105	0.54	0.09
20	C4 – 6815	0.979	−110	0.76	7	1.26	115	0.64	0.08
21	C4 – 6829	0.988	−105	0.88	15	1.36	105	0.66	0.12
22	C4 – 6830	0.988	−105	0.79	2	1.28	120	0.66	0.08
23	C4 – 6831	0.988	−110	0.72	15	1.30	105	0.59	0.09

+ Represents baked emulsion

component of the Balmer and He I lines, giving a systemic velocity of −8 km s^{-1} and a revolution velocity of 17 km s^{-1} for the primary. We refer to these values for correcting the orbital motion of the primary Be star.

3.1. *Radial Velocity*

The radial velocity curves of the Balmer and He I λ3888 shell lines are shown in figures 2a and 2b, respectively. In figure 2b, the full width at half intensity in km s^{-1} for He I λ3888 is also plotted. The radial velocity values of He I λ3888 are the same as those of the Balmer lines, except at phases of around 0.1, where the He I line shows higher values. This is mainly due to the blending with H8, which is 0.4 Å ($\sim$ 30 km s^{-1}) redward of the He I line. Balmer shell lines become very strong at a phase of around 0.1, as shown later. In fact, the full width at half intensity of the He I λ3888 line is larger at these phases ($\sim$ 80 km s^{-1}) than others ($\sim$ 40 km s^{-1}). Except at this particular phase, no systematic differences are seen among the radial velocity curves of Hβ, Hγ, Hδ, and of He I λ3888.

The radial-velocity curves plotted in figures 2a and 2b are generally coincident with those of Poeckert (1981). A hump at a phase of 0.4 to 0.6, which was already noticed by Hynek (1940), Hendry (1970), and Poeckert (1981), can be seen in our curve. The amplitude of the curve is estimated to be about 25 km s^{-1} and the height of the hump is about 15 km s^{-1}.

The radial velocity curves for the Balmer emission peaks are shown in figure 3. The curves of the red and violet peaks run parallel, so that the peak separations are nearly constant through the phase. The amplitude of the curves is estimated to be about 20 km s^{-1}.

3.2. *Emission Intensity*

The V/R values for the Hβ and Hγ lines are plotted in figure 4 as a function of the phase. The V/R variation of ϕ Per is remarkable due to its large amplitude, as high as a factor of 2, and by its clear synchronization with the binary phase, as can be seen in figure 4.

The emission equivalent widths of Hα to Hδ were measured manually as the excess intensities above the interpolated photospheric line profiles. The accuracy of the measurements may be about 10 percent. The results of Hα and Hβ are shown in table 4, and are generally coincident with the values of Poeckert (1981), though ours

Table 2. (Continued)

Table 2-2 Hγ

	Plate No.	Phase	RV_{eb}	I_{eb}	RV_{ac}	I_{ac}	RV_{er}	I_{er}	$\log \frac{I_{eb}}{I_{er}}$
1	C4 – 5927	0.077	−115	0.38	0	0.48	95	0.28	0.13
2	C4 – 5928	0.077	−120	0.48	0	0.50	90	0.28	0.23
3	C4 – 5932	0.077	−90	0.34	0	0.52	90	0.22	0.19
4	C4 – 2264	0.096	−110	0.40	5	0.52	115	0.28	0.16
5	C4 – 2443	0.112	−125	0.34	20	0.40	105	0.37	−0.04
6	C4 – 2473	0.127	−105	0.28	20	0.44	125	0.28	0.00
7	C4 – 4534	0.145	−110	0.42	25	0.40	105	0.32	0.12
8	C4 – 4919	0.190	−95	0.44	25	0.64	160	0.28	0.20
9	C4 – 4920	0.190	−110	0.42	25	0.60	125	0.18	0.37
10	C4 – 4921	0.190	−90	0.52	15	0.64	130	0.28	0.27
11	C4 – 4922	0.190	−90	0.48	15	0.66	110	0.26	0.27
12	C4 – 4923	0.190	−95	0.44	15	0.68	130	0.28	0.20
13	C4 – 4924	0.190	−85	0.44	15	0.66	110	0.28	0.20
14	C4 – 4925	0.191	−85	0.48	15	0.68	135	0.24	0.30
15	C4 – 4929	0.198	−90	0.50	15	0.70	120	0.26	0.28
16	C4 – 4934	0.199	−95	0.38	20	0.72	125	0.24	0.20
17	C4 – 4935	0.199	−90	0.48	20	0.68	130	0.26	0.27
18	C4 – 4936	0.199	−55	0.58	15	0.70	125	0.30	0.29
19	C4 – 2379	0.214	−120	0.32	25	0.66	140	0.28	0.06
20	C4 – 5795	0.221	−95	0.38	25	0.66	120	0.20	0.28
21	C4 – 5800	0.221	−110	0.48	25	0.68	115	0.26	0.27
22	C4 – 2154	0.285	−155	0.40	0	0.80	125	0.38	0.02
23	C4 – 6427	0.422	−120	0.34	−5	0.80	80	0.34	0.00
24	C4 – 6428	0.422	−100	0.38	−12	0.84	85	0.44	−0.07
25	C4 – 6429	0.422	−115	0.30	−7	0.86	105	0.36	−0.08
26	C4 – 6878	0.476	−100	0.28	−5	0.90	75	0.36	−0.11
27	C4 – 6894	0.484	−130	0.30	−5	0.82	65	0.44	−0.17
28	C4 – 5882	0.604	−115	0.28	7	0.72	85	0.48	−0.24
29	C4 – 5884	0.604	−105	0.32	2	0.80	80	0.62	−0.28
30	C4 – 5886	0.605	−120	0.26	−2	0.70	85	0.50	−0.28
31	C4 – 5887	0.605	−115	0.30	5	0.72	80	0.52	−0.24
32	C4 – 6207	0.627	−130	0.22	−15	0.84	75	0.42	−0.28
33	C4 – 6208	0.628	−135	0.24	−20	0.84	70	0.44	−0.26
34	C4 – 7195	0.638	−135	0.18	−15	0.80	80	0.32	−0.25
35	C4 – 7196	0.638	−135	0.28	−5	0.84	75	0.44	−0.19
36	C4 – 6223	0.651	−125	0.24	−17	0.79	70	0.46	−0.28
37	C4 – 6224	0.651	−130	0.26	−10	0.84	75	0.42	−0.21
38	C4 – 6232	0.659	−115	0.28	−7	0.88	75	0.52	−0.27
39	C4 – 6233	0.659	−135	0.30	−25	0.84	70	0.50	−0.22
40	C4 – 5475	0.764	−130	0.20	−20	0.70	90	0.37	−0.27
41	C4 – 5481	0.771	−155	0.38	−25	0.86	75	0.38	0.00
42	C4 – 7104	0.788	−110	0.24	−5	0.90	95	0.30	−0.10
43	C4 – 7105	0.789	−135	0.22	−25	0.88	90	0.22	0.00
44	C4 – 4847	0.954	−120	0.30	−5	0.80	90	0.32	−0.03
45	C4 – 4848	0.954	−110	0.26	−15	0.86	80	0.38	−0.17
46	C4 – 6812	0.979	−125	0.42	25	0.92	115	0.32	0.12
47	C4 – 6814	0.979	−120	0.30	0	0.84	115	0.26	0.06
48	C4 – 6815	0.979	−115	0.36	0	0.90	120	0.28	0.11
49	C4 – 6816	0.979	−115	0.36	0	0.88	130	0.30	0.08
50	C4 – 6817	0.979	−130	0.38	5	0.92	110	0.38	0.00
51	C4 – 6829	0.988	−125	0.34	25	0.84	105	0.24	0.15
52	C4 – 6830	0.988	−130	0.36	10	0.88	115	0.30	0.08
53	C4 – 6831	0.988	−120	0.40	25	0.86	120	0.28	0.16

Table 2. (Continued)

Table 2-3 Hδ

	Plate No.	Phase	RV_{eb}	I_{eb}	RV_{ac}	I_{ac}	RV_{er}	I_{er}
1	C4 – 5927	0.077	−175	0.16	0	0.52	120	0.08
2	C4 – 5928	0.077	−115	0.14	0	0.56	115	0.10
3	C4 – 5932	0.077	−115	0.18	0	0.59	...	0.12
4	C4 – 2264	0.096	−135	0.16	7	0.40	115	0.12
5	C4 – 2265	0.097	−120	0.16	10	0.36	115	0.12
6	C4 – 2442	0.112	−135	0.22	20	0.26	115	0.22
7	C4 – 2443	0.112	−95	0.16	22	0.30	100	0.14
8	C4 – 2473	0.127	−115	0.14	20	0.40	140	0.08
9	C4 – 2474	0.127	−135	0.14	25	0.30	145	0.14
10	C4 – 4533	0.145	−155	0.16	20	0.40	125	0.08
11	C4 – 4534	0.145	−125	0.10	35	0.54	160	0.08
12	C4 – 4919	0.190	−80	0.08	30	0.66	145	0.07
13	C4 – 4920	0.190	−95	0.28	20	0.70	155	0.06
14	C4 – 4921	0.190	−100	0.18	15	0.70	165	0.10
15	C4 – 4922	0.190	−95	0.20	15	0.78	140	0.08
16	C4 – 4923	0.190	−120	0.18	10	0.68	115	0.10
17	C4 – 4924	0.190	−85	0.20	15	0.68	165	0.08
18	C4 – 4925	0.191	−90	0.44	20	0.79	150	0.10
19	C4 – 2364	0.198	−130	0.14	25	0.48	120	0.10
20	C4 – 4929	0.198	−75	0.22	15	0.72	135	0.10
21	C4 – 4934	0.199	−85	0.24	20	0.70	140	0.10
22	C4 – 4935	0.199	−85	0.18	20	0.78	125	0.08
23	C4 – 4936	0.199	−90	0.22	20	0.90	130	0.18
24	C10 – 3253	0.200	−100	0.18	20	0.70	125	0.12
25	C10 – 3254	0.200	−85	0.18	20	0.66	100	0.08
26	C10 – 3263	0.208	−85	0.18	15	0.70	120	0.08
27	C4 – 2379	0.214	−140	0.18	27	0.64	145	0.17
28	C4 – 5800	0.221	−105	0.20	20	0.70	135	0.14
29	C4 – 2154	0.285	−125	0.18	...	0.60	125	0.10
30	C4 – 2155	0.285	−135	0.20	15	0.80	135	0.22
31	C4 – 6424	0.421	−100	0.08	15	0.72	120	0.10
32	C4 – 6425	0.421	−115	0.10	−15	0.78	65	0.08
33	C4 – 6426	0.421	−120	0.14	−10	0.79	115	0.12
34	C4 – 6875	0.476	−110	0.08	...	0.76	80	0.10
35	C4 – 6876	0.476	−140	0.06	−15	0.72	90	0.10
36	C4 – 6895	0.484	−135	0.08	−5	0.78	85	0.14
37	C4 – 5882	0.604	−125	0.12	−5	0.68	110	0.20
38	C4 – 5883	0.604	−150	0.08	5	0.68	95	0.18
39	C4 – 5886	0.605	−135	0.14	10	0.80	95	0.24
40	C4 – 5887	0.605	−125	0.12	5	0.72	100	0.18
41	C4 – 6207	0.627	...	...	−15	0.80	80	0.18
42	C4 – 7195	0.638	−160	0.08	−5	0.70	105	0.10
43	C4 – 6224	0.651	...	...	0	0.80	60	0.26
44	C4 – 6232	0.659	−150	0.06	−15	0.70	85	0.20
45	C4 – 5720	0.755	−165	0.10	−10	0.72	105	0.18
46	C4 – 5474	0.764	−85	0.17	−20	0.70	140	0.20
47	C4 – 5475	0.764	−135	0.14	−25	0.76	75	0.18
48	C4 – 7104	0.788	−95	0.14	−25	0.80	110	0.08
49	C4 – 3102	0.841	−135	0.08	−20	0.80	125	0.16
50	C4 – 4846	0.954	−140	0.17	15	0.80	85	0.16
51	C4 – 4847	0.954	−110	0.12	0	0.76	100	0.10
52	C4 – 6812	0.979	−130	0.02	5	0.70	120	0.04
53	C4 – 6817	0.979	−115	0.06	10	0.70	120	0.04

Table 3. Radial velocity data and equivalent widths for the He I λ3888 shell line of φ Per.

	Plate No	Phase	I_{ab}	RV_{ac}	I_{ac}	I_{ar}	E.W. (Å)	F.W. (km s^{-1})
1	C4 – 2264	0.096	0.90	28	0.32	0.80	0.37	85
2	C4 – 2265	0.097	0.90	28	0.34	0.88	0.35	80
3	C4 – 2442	0.112	0.82	55	0.22	0.80	0.38	85
4	C4 – 2443	0.112	0.84	53	0.28	0.84	0.37	85
5	C4 – 2473	0.127	0.80	40	0.40	0.82	0.25	80
6	C4 – 2474	0.127	0.80	40	0.30	0.80	0.37	85
7	C4 – 4533	0.145	0.84	28	0.32	0.84	0.28	70
8	C4 – 4534	0.145	0.80	45	0.26	0.80	0.36	75
9	C4 – 4919	0.190	0.84	23	0.40	0.80	0.20	35
10	C4 – 4920	0.190	0.84	23	0.44	0.84	0.16	50
11	C4 – 4921	0.190	0.86	25	0.40	0.80	0.17	40
12	C4 – 4922	0.190	0.84	18	0.40	0.80	0.16	35
13	C4 – 4923	0.190	0.80	18	0.40	0.82	0.13	30
14	C4 – 4924	0.190	0.90	18	0.44	0.88	0.18	45
15	C4 – 4925	0.190	0.82	18	0.44	0.88	0.18	40
16	C4 – 2364	0.198	0.82	48	0.38	0.82	0.25	60
17	C4 – 4929	0.198	0.84	23	0.40	0.86	0.22	35
18	C4 – 4934	0.199	0.86	23	0.40	0.84	0.20	30
19	C4 – 4935	0.199	0.86	28	0.40	0.86	0.20	30
20	C4 – 4936	0.199	0.82	23	0.40	0.84	0.21	30
21	C10 – 3253	0.200	0.82	23	0.38	0.80	0.15	35
22	C10 – 3254	0.200	0.82	23	0.28	0.84	0.19	30
23	C10 – 3263	0.208	0.82	23	0.39	0.80	0.19	30
24	C10 – 3264	0.208	0.92	28	0.30	0.80	0.26	25
25	C4 – 2379	0.214	0.84	43	0.42	0.84	0.20	65
26	C4 – 5800	0.221	0.92	23	0.50	0.88	0.23	40
27	C4 – 2154	0.285	0.84	30	0.52	0.80	0.37	...
28	C4 – 2155	0.285	1.00	30	0.54	1.00	0.37	...
29	C4 – 6424	0.421	0.86	−12	0.36	0.84	0.17	40
30	C4 – 6425	0.421	0.84	−12	0.38	0.80	0.14	35
31	C4 – 6426	0.421	0.84	−12	0.38	0.80	0.15	35
32	C4 – 6875	0.476	0.82	−7	0.50	0.82	0.12	45
33	C4 – 6876	0.476	0.84	−2	0.50	0.84	0.16	40
34	C4 – 6895	0.484	0.86	−2	0.50	0.86	0.13	45
35	C4 – 5882	0.604	0.80	3	0.44	0.86	0.12	40
36	C4 – 5883	0.604	0.84	8	0.44	0.86	0.16	45
37	C4 – 5886	0.605	0.80	8	0.44	0.84	0.14	35
38	C4 – 5887	0.605	0.88	5	0.46	1.00	0.18	35
39	C4 – 6207	0.627	0.86	−9	0.50	0.92	0.15	40
40	C4 – 7195	0.638	0.84	3	0.58	0.88	0.10	45
41	C4 – 6224	0.651	0.82	−7	0.44	0.86	0.15	35
42	C4 – 6232	0.659	0.80	−7	0.58	0.82	0.08	45
43	C4 – 5720	0.755	0.80	−17	0.40	0.82	0.13	35
44	C4 – 5474	0.764	0.84	−17	0.42	0.86	0.17	40
45	C4 – 5475	0.764	0.86	−17	0.46	0.86	0.15	45
46	C4 – 7104	0.788	0.82	−17	0.52	0.82	0.09	40
47	C4 – 3102	0.841	0.88	...	0.68	0.88	0.11	...
48	C4 – 4846	0.954	0.80	−12	0.44	0.80	0.22	45
49	C4 – 4847	0.954	0.82	−7	0.50	0.80	0.19	55
50	C4 – 6812	0.979	0.84	−7	0.62	0.84	0.16	...
51	C4 – 6816	0.979	0.86	−17	0.68	0.84	0.12	...
52	C4 – 6817	0.979	0.82	−12	0.70	0.80	0.08	...

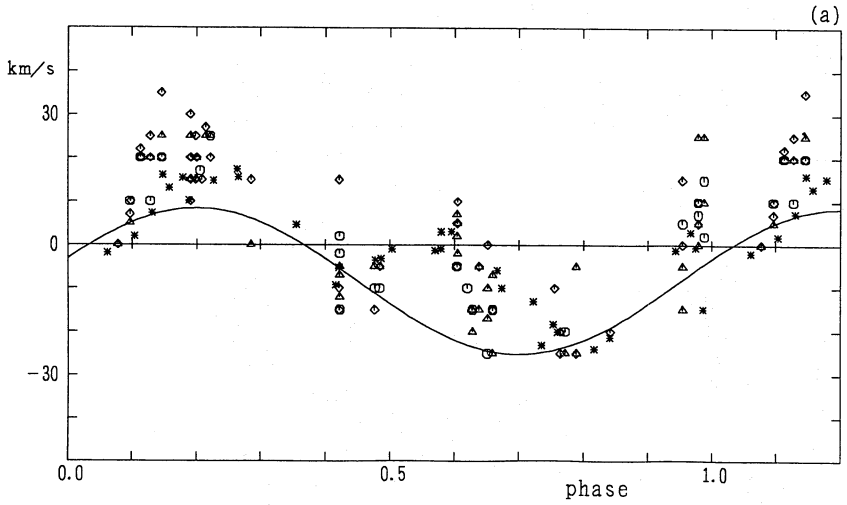

Fig. 2a. Plot of the radial velocity against the phase for the Balmer shell lines. The velocities of Hβ are designated by open circles, Hγ by triangles, Hδ by diamonds, and those of Poeckert (1981) by asterisks. The solid line represents Poeckert's (1981) orbital solution for the primary star.

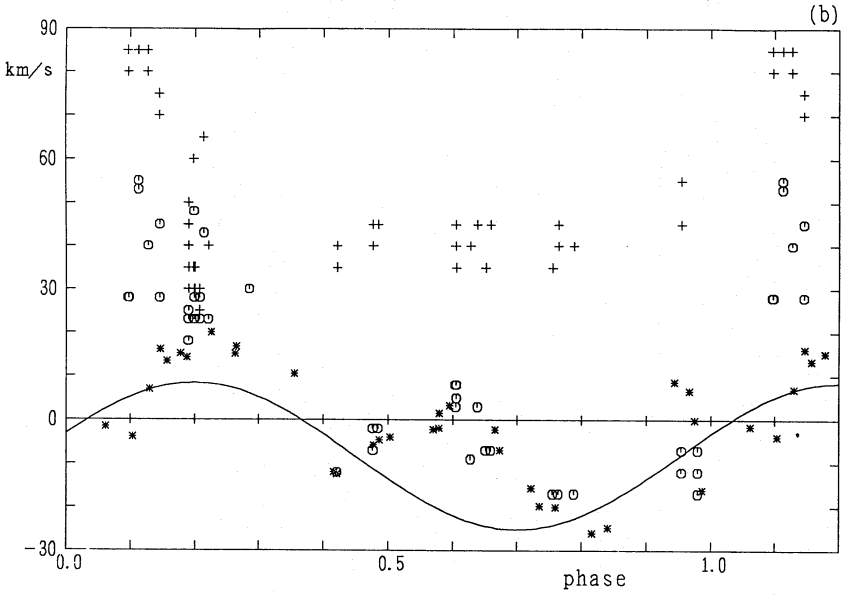

Fig. 2b. Radial velocity and line width for the He I λ3888 shell line. Our measurements of velocities are designated by open circles, and those of Poeckert (1981) by asterisks. The full width at half intensity is shown by a plus sign.

are slightly higher on the average.

3.3. Shell Intensity

The phase dependence of the highest member of the Balmer lines traceable as shell absorption is plotted in figure 5 for our case and that of Lockyer (1926). The duration of the strong shell phase is almost the same for both cases, suggesting a stable state for the shell-line forming region in the envelope. In figure 5 is also marked the strong shell phase of He I λ4471, which is taken from Poeckert (1981). The appearance of the strong shell phase is just opposite for Balmer and He I lines with each other.

In figure 5, one may notice that the highest level of H_n outside the strong shell phase is generally higher in

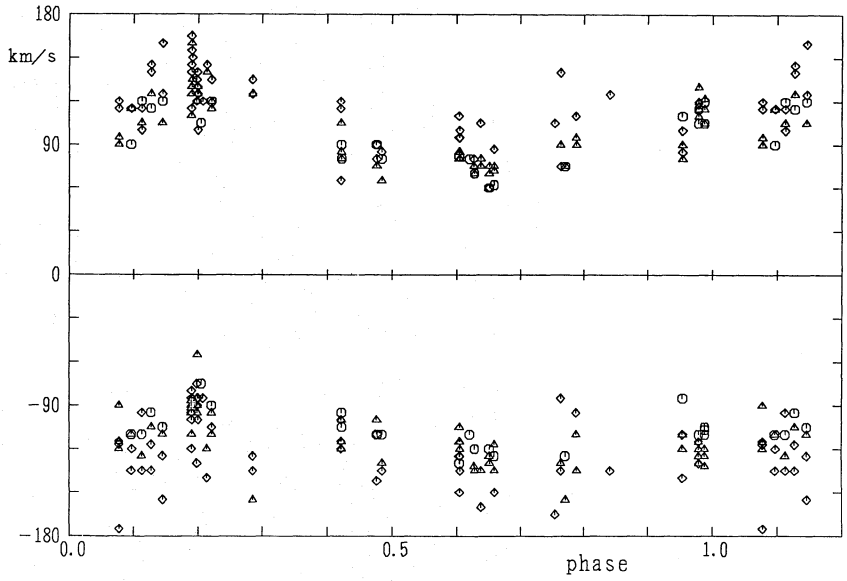

Fig. 3. Plot of the radial velocity against the phase for the Balmer emission peaks. The velocities of Hβ are designated by open circles, Hγ by triangles, and Hδ by diamonds.

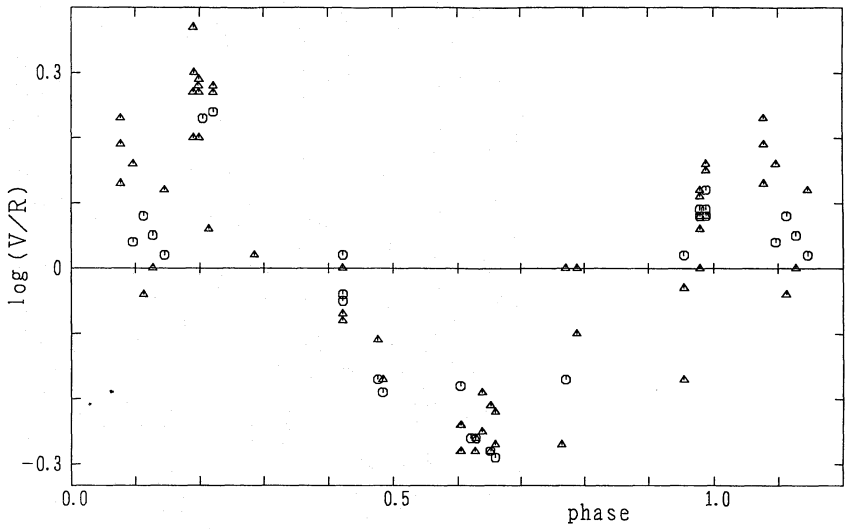

Fig. 4. Plot of the intensity ratio of the violet to red emission peaks (V/R) against the phase. The V/R ratios of Hβ are designated by open circles and those of Hγ by triangles.

Lockyer's data (1926) ($n \sim 10$) than in ours ($n \sim 6$). If this difference is true, the envelope must have been more opaque in the epoch of Lockyer's data than ours.

3.4. Phase Dependence

When combined with the existing data of Lockyer (1926), Poeckert (1981), and others, sufficient phase-locked variations are seen in the following behavior:

(a) The appearance of a hump in the radial-velocity curves of the Balmer and He I shell lines at a phase of 0.4 to 0.6.

(b) The V/R ratios in the Hβ and Hγ emission profiles.

(c) The appearance of a strong shell phase in the Balmer lines at a phase of 0.05 to 0.15.

A strong shell phase in He I, which was noticed by Poeckert (1981), was not confirmed because of a low signal-to-noise ratio in our spectrograms.

Table 4. Equivalent widths of the Balmer emission lines.

Hα

Phase	0.097	0.112	0.128	0.285	0.605	0.637	0.764	0.841	0.954
E.W. (Å)	80	59	49	51	73	51	68	48	62

Hβ

Phase	0.096	0.112	0.127	0.145	0.205	0.221	0.422	0.422	0.422	0.476	0.484	0.604
E.W. (Å)	3.8	3.6	3.7	4.5	4.0	4.5	4.2	4.1	4.5	4.4	4.1	4.4

Phase	0.620	0.628	0.651	0.659	0.771	0.954	0.979	0.979	0.988	0.988	0.988
E.W. (Å)	4.0	4.8	4.4	4.5	4.1	4.2	4.1	2.2	3.2	3.9	3.9

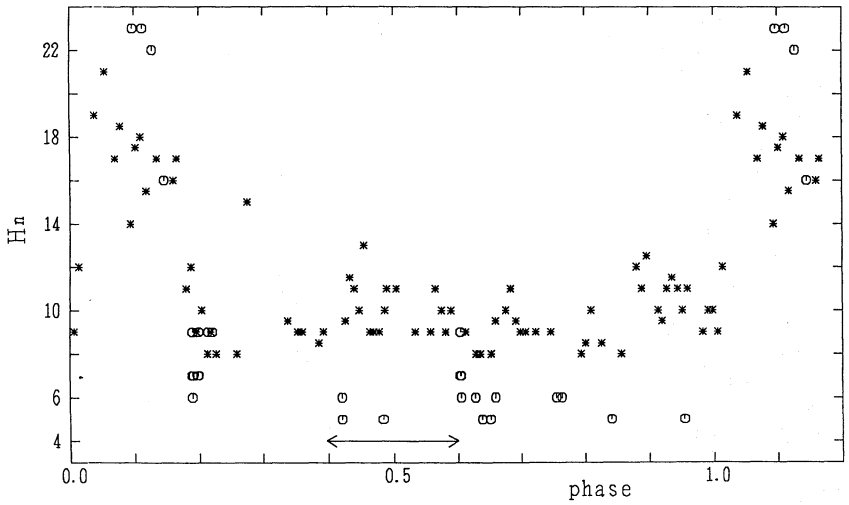

Fig. 5. Plot of H_n (the highest member of Balmer hydrogen lines seen as shell absorption) against the phase. Our measurements are designated by open circles, and those of Lockyer (1926) by asterisks. The strong shell phase of He I λ4471 (Poeckert 1981) is indicated by the arrow.

On the other hand, no clear phase dependence has been found in the emission-equivalent widths and the peak separations of the Balmer emission lines.

The orbital phase-locked behavior in (a) and (b) are related to the structure of the absorbing and emitting envelopes, respectively. The behavior described in (c) is related to the inhomogeneity inside the envelope. Phase-independent quantities, such as the emission equivalent width and the peak separation, indicate that the emitting envelope is stable in the binary system without showing a significant change in the volume emission measure as well as in the size of the envelope.

4. Binary Masses

The mass and mass ratio of the binary components are the basic parameters used for studying the envelope structure in binary systems. The size of the envelope and the motion of gas in the envelope are notably affected by these binary parameters. Suzuki (1980) and Poeckert (1981), starting from different methods of approach, have arrived at similar binary masses, about 20 $M_\odot$ and 4 $M_\odot$ for the primary and the secondary, respectively. Their arguments, however, may have some problems which need to be re-examined as follows.

4.1. Suzuki's Case

Suzuki (1980) has calculated the periodic stable orbits of the restricted three-body problem and applied them to the envelope around the primary Be star in the ϕ Per system. The envelope extends perpendicular to the axis connecting the primary and secondary in the orbital plane of the system.

He assumed that the emission and absorption lines

both originate from ionized gas orbiting in these periodic stable orbits. The hump seen in the radial velocity curves of the shell lines, as well as the double-periodicity of the emission edge velocities (Hynek 1940), were both explained as being the result of a superposition of the revolutional motion of a non-circular envelope in the system, and the rotational motion of the gas in the envelope around the Be star.

Comparing the theoretical radial velocity curves with the observed curves derived from Hynek's (1940) data, Suzuki has obtained the binary parameters, including the masses of 20 $M_\odot$ and 4 $M_\odot$ for the primary and secondary, respectively.

However, the radial-velocity curves of Hynek (1940) both in shell lines and emission edges are to be re-examined for the purpose of comparing them with Suzuki's (1980) model calculation.

First, the radial-velocity curves of the shell lines in our measurements, which are in good agreement with those of Poeckert (1981), reveal an amplitude of around 10 km s^{-1} lower than in the case of Hynek (1940). We measured the velocities of the shell lines at their deepest core, assuming that the core velocities yield the motion of the most effectively absorbing layers. Since the shell lines often exhibit marked asymmetric profiles, the velocity measurements may depend sensitively on the position of bisection in the shell line profiles.

Second, Suzuki adopted the radial velocities of Hynek's (1940) emission edges by regarding them as being the values of the emission peaks. The actual emission peak velocity is much smaller than the velocity at the emission edge. Our measurements reveal that the emission-peak velocities are more than 50 km s^{-1} smaller than Suzuki's adopted values.

Following Suzuki's (1980) method, but adopting our new values for the radial velocities, we have failed to find any reasonable combination of the binary masses in his calculations. This is mainly due to the drastically reduced values of the emission-peak velocity. Extrapolating Suzuki's (1980) calculations given in his figures, it is possible that the observed radial velocities can be explained in the smaller mass binary system.

The emission-peak separation is a good indicator of the outer radii of the emission envelopes (Hirata, Kogure 1984). Assuming a primary mass of 20 $M_\odot$, the observed small peak separation suggests that the formation region of the Balmer emission lines extends beyond the inner Roche lobe. Moreover, since the deformation of this periodic stable envelope is small, it is difficult to explain the large V/R values observed in the Balmer lines. For these reasons, it is not suitable to apply his model in its original form to determine the binary masses using the velocities of the Balmer lines.

4.2. Poeckert's Case

Poeckert (1981) has derived masses of 21 $M_\odot$ and 3.4 $M_\odot$ for the primary and secondary, respectively, based on the revolution velocities of the binary components. He used the broad photospheric Balmer and He I lines for the primary, and the center of the He II emission line (λ4686) for the secondary. Though his derived masses are very close to those of Suzuki (1980), it is not appropriate to use the He II lines to measure the revolution velocity of the secondary. This is because the He II emission line also exhibits a V/R variation synchronized to the binary period, as Poeckert (1981) himself pointed out. This V/R variation implies that the envelope of the secondary must be elongated toward the primary, and that the elongation causes a shift in the center of the emission line profile in the same direction as the orbital motion of the secondary.

Then, the real revolution velocity of the secondary should be smaller than that measured by Poeckert (1981). If the revolution velocity of the secondary were to be reduced by 10 percent from his value, i.e. $K_2 = 95$ km s^{-1} and $K_1 = 17$ km s^{-1}, the binary masses would be reduced to about 15 $M_\odot$ and 2.5 $M_\odot$. If reduced by 20 percent, i.e. $K_2 = 80$ km s^{-1} and $K_1 = 17$ km s^{-1}, the masses would be about 10 $M_\odot$ and 2 $M_\odot$. Though the actual size of the velocity reduction is not known, it is very possible that the binary masses are smaller than the current values.

5. Envelope Structure

ϕ Per is a typical V/R variable. The V/R ratio shows a periodic variation with a binary period of 126.696 d. The curves of the radial velocities of the emission peaks and of the shell absorption are parallel to that of the V/R variation, as can be seen in figures 2, 3, and 4, while the radial-velocity curves of the shell absorption lines show a hump. When the V/R ratio exceeds unity, i.e. the violet component is stronger, the radial velocities always shift towards the positive, and vice versa.

The V/R variation has so far been explained either in terms of an axisymmetric rotating pulsating envelope, or in terms of the apsidal motion of an elliptical disk (Hubert et al 1987; Ballerau, Chauville 1989). We discuss the envelope structure of ϕ Per based on the following facts:

(1) The variation of the radial velocities and V/R are locked in the binary phase.

(2) The V/R variation shows a large amplitude of up to ~ 2.

(3) The amplitudes of the radial velocity curves are relatively small (~ 5 to 10 km s^{-1}).

The observed radial velocities are a combination of the rotational motion around the primary and the revolutionary motion in the system. When the revolutionary

Table 5. Elliptic ring parameters (e) and (a) derived from the Balmer emission lines.

Line	Blue peak (km s^{-1})	Red peak (km s^{-1})	Peak separation (km s^{-1})	e	a ($R_\odot$)		
phase = 0.2							
Hβ	−95	105	200	0.05	382	287	191
Hγ	−105	110	215	0.02	330	248	165
Hδ	−110	120	230	0.04	289	217	144
phase = 0.7							
Hβ	−100	95	195	0.03	401	301	201
Hγ	−110	100	210	0.05	347	260	173
Hδ	−115	110	225	0.02	302	226	151
					M_*= 20$M_\odot$	15$M_\odot$	10$M_\odot$

motion is corrected, using the orbital parameters given by Poeckert (1981), the amplitudes of the radial-velocity curves are about 5 km s^{-1} for the emission peaks, and about 10 km s^{-1} for the shell lines.

Some binary Be stars show binary phase-locked V/R variations. Among them, HR 2142 (Peters 1972), 4 Her (Harmanec et al 1976) and 88 Her (Doazan et al 1982a,b) are well observed, despite their V/R values not being so large. The V/R ratio ranges from 0.8 to 1.0 for HR 2142, 0.95 to 1.2 for 4 Her, and 0.9 to 1.15 for 88 Her. The V/R ratio up to 2 observed in the ϕ Per system is then of a unique nature among binary Be stars.

We first consider the V/R variation observed in the ϕ Per system under the assumption of the elliptic disk model. If the orientation of the elliptic disk is locked in the Roche lobe of the primary, the phase-locked behavior is a natural consequence. We derive the envelope parameters based on the elliptical disk model formulated by Huang (1973) and Mon (1984). According to this model, the semi-major axis a (a measure of envelope extension) and eccentricity e (a measure of elongation) were calculated and are given in table 5.

Their formulation is applicable when the major axis of an elliptic disk is perpendicular to the line of sight, corresponding to phases of 0.2 and 0.7 in the ϕ Per system. The peak velocities shown in the table are the values after correcting for the revolutionary motion in the system. It is to be noticed that the value of the semi-major axis depends on the mass of the primary component. Since the mass of a B2 V star is ordinarily around 10 $M_\odot$ (Underhill, Doazan 1982) and the primary mass is possibly smaller than 20 $M_\odot$ (see section 4), we calculated for three cases of 20 $M_\odot$, 15 $M_\odot$, and 10 $M_\odot$. The value of $\sin i$ was set to be unity because of the large $V \sin i = 450$ km s^{-1}.

The calculated e values (0.02–0.05) show that the envelope extends slightly farther in the direction facing the secondary. It is difficult to explain the large values of V/R $\sim$ 2 using an elliptic disk model with such a small scale of asymmetry.

Castle (1977) calculated the stability of the elliptic rings in binary systems, and showed the possible apsidal motion of these elliptic rings. She has applied the calculations to the long-term V/R variation in ζ Tau, finding a reasonable solution. However, since the phase-locked variation is ruled out in her calculations, her model is hardly applicable to the ϕ Per system.

On the other hand, in the frame of a pulsating envelope, a V/R value not equal to unity is due to the asymmetry of a velocity field introduced by the expanding or contracting motion. As the amplitudes of the radial velocity of the emission peaks or of the shell absorption lines, after correcting for the orbital motion of the primary, are around 10 km s^{-1}, the expanding or contracting motions in the envelope are expected to be of the same order, that is, several tens of km s^{-1}. The rotational motions in the envelope may be several hundred km s^{-1} because $V \sin i = 450$ km s^{-1}. The asymmetry of the velocity field caused by this small pulsation velocity is so small that a large V/R ratio cannot be expected. According to the calculations carried out by Poeckert, Marlborough (1978), a profile having a sufficiently large V/R ratio is formed in the envelope where the expanding velocity reaches around 100 km s^{-1} or more. Moreover, the pulsation model needs an additional reason for the synchronization of the pulsation period with the binary orbital motion.

In this way, both the model of an elliptic disk and that of a pulsating envelope have met with serious difficulties in consistently explaining the characteristic behaviors of the V/R variations, (1) through (3) cited above. In order to overcome these difficulties, the following points should be emphasized:

(a) The reliable determination of the binary parameters.

(b) Possible effects on the envelope structure, such as the extension of the whole envelope, mass concentration

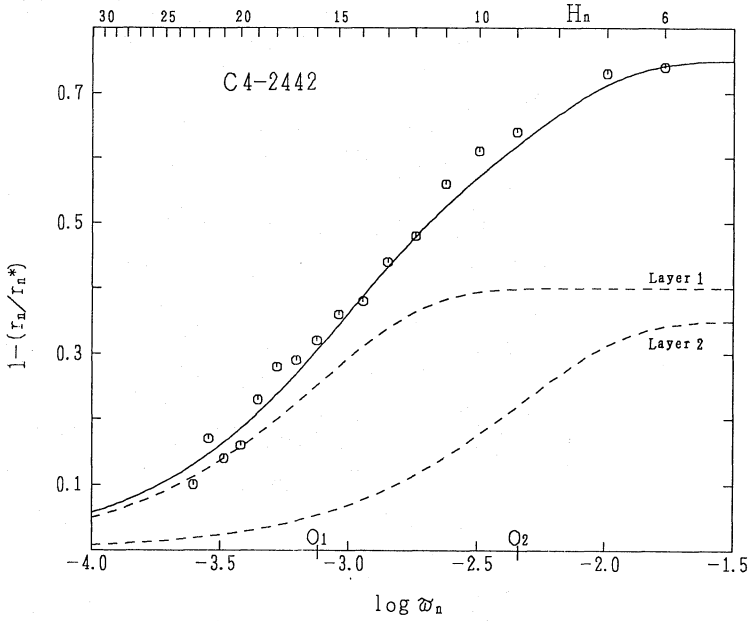

Fig. 6. Fitting of the residual intensities for the plate C4-2442. The dashed lines denote the curves for layers 1 and 2. The solid curve represents a composite theoretical curve which can be compared with the observed points (open circle). On the lower abscissa, the points of $\log \varpi_n = 0$ for each layer are indicated by O_1 and O_2. The upper abscissa gives the position of the Hn lines on the $\log \varpi_n$ coordinate.

inside the envelope, and even the multiple structure in the system.

Further spectroscopic observations with a higher signal-to-noise ratio and fully covering the binary phase are required.

As for the extension of the envelope, the calculated a values given in table 5 suggest the possibility of its large extension, exceeding the Roch lobe. Kogure et al (1992) discussed the envelope extension of several binary Be stars and obtained the same result for ϕ Per.

The large values of the equivalent width of the Hα emission in the range of 40 to 60 Å (table 4) are remarkable when we consider the small optical depth of τ (Hα) < 100 for the Hα envelope, except in the strong shell phase in the hydrogen spectrum, which is given in the next section. The strong emission and small optical depth of the Hα line imply that the envelope should be extended vertically above and below the orbital plane of the binary system (Kogure 1990).

6. Strong Shell Phase

As already noticed, ϕ Per is generally a weak shell star showing shell absorption features only for lower Balmer ($<$ H$_7$) and He I λ3888 lines. Lockyer (1926) first noticed that the hydrogen shell lines became conspicuous at a particular phase of 0.05 to 0.15, where the shell absorption feature can be traced up to H$_{23}$ or so. This strong shell phase is also confirmed in our spectrograms. Brown (1992) reported an abrupt minima of about 0.1 mag in the V band at phases of around 0.1 and 0.5, which correspond to the strong shell phases of the hydrogen and helium lines, respectively. It is apparent from these observations that there are density enhancements in the envelope in the regions seen at these particular phases.

6.1. β, τ Analysis

We now proceed to the central depth analysis of Kogure et al (1978) for shell lines in the strong shell phase, for which we have used 3 plates (C4–2265, C4–2442, and C4–2474) for the measurements.

There is no significant Balmer progression, as seen in table 6, for hydrogen shell lines. We therefore adopted Hirata, Kogure's (1977) expressions to determine the optical thickness in Hα radiation (τ(Hα)) and the fraction of the star's surface screened by the envelope (β),

$$1 - \frac{r_n}{r_{n^*}} = \beta\,[1 - \exp(-\varpi_n \tau(\mathrm{H}\alpha))], \qquad (1)$$

where r_n and r_{n*} are the central residual intensities of the shell absorption component and of the broad stellar absorption of the H$_n$ line, respectively, and $\varpi_n = \dfrac{\nu_{2n} B_{2n}}{\nu_{23} B_{23}}$. B_{2n} and B_{23} are the Einstein coefficients.

Table 6. Radial velocity and central residual intensities of the shell lines of ϕ Per.

	C4–2265				C4–2442				C4–2474			
H_n	RV km s^{-1}	r_n	r_{n^*}	$1-\frac{r_n}{r_{n^*}}$	RV km s^{-1}	r_n	r_{n^*}	$1-\frac{r_n}{r_{n^*}}$	RV km s^{-1}	r_n	r_{n^*}	$1-\frac{r_n}{r_{n^*}}$
6	20	0.36	0.94	0.61	20	0.24	0.92	0.74	20	0.30	0.88	0.66
7	10	0.38	0.90	0.57	20	0.22	0.84	0.73	25	0.32	0.86	0.62
9	15	0.48	0.92	0.48	30	0.30	0.84	0.64	25	0.42	0.84	0.50
10	15	0.48	0.92	0.48	20	0.34	0.88	0.61	25	0.54	0.84	0.35
11	20	0.60	0.98	0.38	30	0.40	0.92	0.56	25	0.58	0.90	0.35
12	25	0.70	0.98	0.28	25	0.50	0.98	0.48	30	0.58	0.92	0.37
13	25	0.72	1.00	0.28	35	0.56	1.00	0.44	35	0.70	1.00	0.30
14	15	0.72	1.00	0.28	35	0.62	1.00	0.38	27	0.76	1.00	0.24
15	20	0.79	1.00	0.21	20	0.64	1.00	0.36	27	0.72	1.00	0.28
16	17	0.68	0.92	0.26	20	0.68	1.00	0.32	35	0.78	1.00	0.22
17	12	0.74	0.98	0.24	25	0.72	1.02	0.29	35	0.72	1.00	0.28
18	12	0.78	0.96	0.18	32	0.72	1.00	0.28	37	0.80	1.00	0.20
19	35	0.82	1.00	0.18	27	0.78	1.02	0.23	25	0.84	1.00	0.16
20	25	0.88	1.00	0.12	10	0.84	1.00	0.16	...	0.88	1.00	0.12
21	15	0.88	1.02	0.13	25	0.86	1.00	0.14	20	0.82	1.00	0.18
22	30	0.92	1.04	0.11	35	0.88	1.06	0.17	32	0.82	1.00	0.18
23	10	0.96	1.04	0.07	10	0.90	1.00	0.10	...	...	...	...

In the case of ϕ Per, two combinations of $(\beta_1, \tau_1(\mathrm{H}\alpha))$ and $(\beta_2, \tau_2(\mathrm{H}\alpha))$ were applied and $\tau_1(\mathrm{H}\alpha) > \tau_2(\mathrm{H}\alpha)$ can be taken without any loss of generality. We use layers 1 and 2 for the layers characterized by the combination of $\beta_1, \tau_1(\mathrm{H}\alpha)$ and $\beta_2, \tau_2(\mathrm{H}\alpha)$, respectively. Then, equation (1) is written as

$$1-\frac{r_n}{r_{n^*}} = \beta_1[1-\exp(-\varpi_n\tau_1(\mathrm{H}\alpha))] + \beta_2[1-\exp(-\varpi_n\tau_2(\mathrm{H}\alpha))]. \quad (2)$$

The results of the measurement for r_n and r_{n^*} are given in table 6, where the radial velocities (RV) of the hydrogen shell lines are also shown to check that there is no Balmer progression. An estimation of the β's and τ's in the case of C4–2442 is illustrated in the figure 6. The estimated values of $(\beta_1, \tau_1(\mathrm{H}\alpha))$ and $(\beta_2, \tau_2(\mathrm{H}\alpha))$ are presented in table 7. Outside the strong shell phase, the highest number of observed Balmer shell lines is 6 or so, which means that the optical thickness in Hα is much smaller than 100.

6.2. *Electron Density in the Strong Shell Phase*

The optical depth $\tau(\mathrm{H}\alpha)$ is calculated from the equation

$$\tau(\mathrm{H}\alpha) = \frac{h\nu_{23}}{4\pi}B_{23}N_2(R_2-R_1), \quad (3)$$

where ν_{23} and B_{23} denote the frequency and Einstein coefficient of the 2-to-3 transition, respectively, N_2 the averaged population of hydrogen atoms in the second level in the envelope, R_2 the envelope outer extension, and R_1 the inner radius of the envelope assumed to be the stellar radius R_*.

For the averaged population N_2, we adopt the formulation given by Kogure (1959). The related physical values are taken from his table, considering $T_{\mathrm{eff}} = 22,000$ K, since ϕ Per is a B2 IVep-type star (Gies, Lambert 1992).

Setting R_2 to r times R_* and assuming that $r >> 1$, the electron density (N_e) and the column density ($N_\mathrm{e}H$) at the strong shell phase are expressed as

$$N_\mathrm{e} \simeq \frac{3.26\times10^{16}}{\sqrt{R_*}}\frac{\sqrt{\tau(\mathrm{H}\alpha)}}{r\sqrt{r}}\left(1-\frac{1}{2r}\right) \quad (4)$$

and

$$N_\mathrm{e}H \simeq 3.26\times10^{16}\sqrt{R_*}\frac{\sqrt{\tau(\mathrm{H}\alpha)}}{\sqrt{r}}\left(1-\frac{3}{2r}\right). \quad (5)$$

We have calculated these values in two cases of the stellar radius, $R_* = 15R_\odot$ (Poeckert 1981) and $R_* = 6R_\odot$ (Underhill, Doazan 1982); the results are given in table 7 for three values of the outer radius.

In the mass-concentrated region, the electron density takes a value of (1–10) $\times 10^{10}$ cm^{-3}, though it depends on its extension. This is similar to typical shell stars (Kogure et al 1978). Outside this strong shell phase, the electron density is estimated to be 10-times smaller.

It is curious, however, that the effect of this high-density region is not seen on the V/R variations. There probably exists another enhanced density region, where

Table 7. Physical parameters derived from the shell absorption lines.

(a) Column density

Plate	Layer	β	log τ (Hα)	$R_* = 6R_\odot$ $r = 5$	$r = 10$	$r = 15$	$R_* = 15R_\odot$ $r = 3$	$r = 5$	$r = 7$
C4–2265	Layer 1	0.30	3.08	2.29(23)	1.97(23)	1.70(23)	3.34(23)	3.62(23)	3.43(23)
	Layer 2	0.30	2.31	9.42(22)	8.09(22)	7.00(22)	1.37(23)	1.49(23)	1.41(23)
C4–2442	Layer 1	0.40	3.12	2.41(23)	2.06(23)	1.78(23)	3.49(23)	3.78(23)	3.59(23)
	Layer 2	0.35	2.34	9.75(22)	8.38(22)	7.24(22)	1.42(23)	1.54(23)	1.46(23)
C4–2474	Layer 1	0.40	3.31	2.98(23)	2.55(23)	2.21(23)	4.34(23)	4.71(23)	4.47(23)
	Layer 2	0.30	2.30	9.32(22)	8.00(22)	6.92(22)	1.36(23)	1.47(23)	1.40(23)

(b) Electron density

Plate	Layer	β	log τ (Hα)	$R_* = 6R_\odot$ $r = 5$	$r = 10$	$r = 15$	$R_* = 15R_\odot$ $r = 3$	$r = 5$	$r = 7$
C4–2265	Layer 1	0.30	3.08	1.41(11)	5.26(10)	2.91(10)	1.78(11)	8.90(10)	5.55(10)
	Layer 2	0.30	2.31	5.80(10)	2.16(10)	1.20(10)	7.31(10)	3.67(10)	2.29(10)
C4–2442	Layer 1	0.40	3.12	1.47(11)	5.50(10)	3.05(10)	1.85(11)	9.32(10)	5.80(10)
	Layer 2	0.35	2.34	5.55(10)	2.24(10)	1.24(10)	7.57(10)	3.80(10)	2.36(10)
C4–2474	Layer 1	0.40	3.31	1.83(11)	6.85(10)	3.80(10)	2.31(11)	1.16(11)	7.23(10)
	Layer 2	0.30	2.30	5.74(10)	2.15(10)	1.19(10)	7.23(10)	3.63(10)	2.26(10)

the He I shell lines are strengthened. How the mass-concentrated regions are formed and kept in the envelope and why the strengthened lines are different (H I and He I) in the two regions are problems which need to be solved.

In a mass-exchanging binary with an inner Roche lobe overflow from the secondary to the primary through point L_1, two enhanced density regions in the accretion disk around the primary are formed according to the calculations, say, by Matsuda et al (1990). This is very attractive for understanding the two strong shell phases observed in the ϕ Per system, though there is no clear evidence of mass transfer.

7. Summary

Based on our newly measured data combined with previous studies, we have examined the envelope structure around the primary of the ϕ Per system.

We have measured the radial velocities and line intensities at some characteristic points of the Balmer and He I lines. We have thus confirmed the phase-dependent variation of the V/R ratio and the phase-locked behavior, such as the hump in the radial-velocity curves of the Balmer and He I (λ3888) shell lines and the strong shell phase in the Balmer lines. These suggest that the Be envelope around the primary is stable in the ϕ Per system.

We have criticized the previous binary models of Suzuki (1980) and Poeckert (1981). Both models are found to have respective difficulties in determining the binary masses, mainly due to the reason that the formation regions of the Balmer and He II emission lines are not specified. Our arguments concerning these models suggest that the binary masses are probably smaller than their values.

Two envelope models have so far been proposed for explaining the V/R variablities, an axisymmetric rotating pulsating envelope and an apsidal motion of an elliptical disk. Both models, however, are found to be unsuccessful in simultaneously explaining the large amplitude of the V/R variation and the small amplitude of the radial-

velocity curves of the Balmer lines observed in ϕ Per.

One possibility is to consider a highly efficient emitting region, say, by mass concentration, in the part of the envelope facing the secondary. Such a region, if it exists, must influence the formation of shell lines in the binary phase around 0.5. It is not certain whether this region is responsible for the formation of the strong He I shell lines given below.

The strong shell absorption lines are observed at limited phases, which suggests an inhomogeneity in the envelope. This is supported by photometric observations (Brown 1992). In the ϕ Per system, the Balmer lines are strengthened at a phase of around 0.1 and the He I lines at a phase of around 0.5, which poses the question of the physical conditions in the envelope. The binary interaction, the mass flow from the secondary, may cause an inhomogeneity in the envelope around the primary (Matsuda et al 1990), though no evidence of mass flow has been reported.

The small amplitude of the radial-velocity curve and the small peak separation of the Balmer emission lines suggest the possibility that a common envelope exists outside the Roche lobe, and also that the envelope around the secondary may contribute to the formation of Balmer emission profiles. If so, the resultant profiles may become complicated and possibly show some dependence on the binary phase. The profiles given by Poeckert (1981) show, indeed, much fine structure in the Balmer emission lines as well as in the emission lines of He I and metals. An examination of this fine structure will provide much information concerning the envelope structure in the ϕ Per system.

Further spectroscopic observations with a high signal-to-noise ratio and fully covering the binary phase are essential.

The authors wish to express their hearty thanks to the staff members of Okayama Astrophysical Observatory for their help during the observations. They are also thankful to Prof Y. Nakai and Dr K. Iwasaki, Kwasan Observatory, Kyoto University for helping during the PDS measurements. One of the authors, Mahendra Singh, is very much thankful to the Inoue Foundation for Science, Tokyo, for providing the financial support to carry out the research in Japan.

References

Ballereau D., Chauville J. 1989, A&A 214, 285
Brown C.F. 1992, PASP 104, 38
Campbell W.W. 1902, ApJ 16, 114
Castle K.G. 1977, PASP 89, 862
Delplace A.M. 1970a, A&A 7, 68
Delplace A.M. 1970b, A&A 7, 459
Doazan V., Harmanec P., Koubsky J., Krpata J., Zdarsky F. 1982a, A&AS 50, 481
Doazan V., Harmanec P., Koubsky J., Krpata J., Zdarsky F. 1982b, A&A 115, 138
Gies D.R., Lambert D.L. 1992, ApJ 387, 673
Harmanec P., Koubsky J., Krpata J., Zdarsky F. 1976, Bull Astron Inst Czech 27, 47
Harmanec P. 1984, Bull Astron Inst Czech 35, 164
Hendry E.M. 1970, in Be and Shell Stars, IAU Symp. No.70, ed A. Slettebak (Reidel, Dordrecht) p429
Hickok F.R. 1969, MSc Thesis, University of Toronto
Hirata R., Kogure T. 1977, PASJ 29, 477
Hirata R., Kogure T. 1984, Bull Astron Soc India 12, 109
Huang S.-S. 1973, ApJ 183, 541
Hubert A.M., Floquet M., Chambon M.T. 1987, A&A 186, 213
Hynek J.A. 1940, Contr Perkins Obs 14
Hynek J.A. 1944, ApJ 100, 151
Kogure T. 1959, PASJ 11, 278
Kogure T. 1990, Ap&SS 163, 7
Kogure T., Hirata R., Asada Y. 1978, PASJ 30, 385
Kogure T., Mon M., Suzuki M., Singh M. 1992, PASPC 38, 404
Lesh J.R. 1968, ApJS 17, 371
Lockyer W.J.S. 1925, MNRAS 85, 580
Lockyer W.J.S. 1926, MNRAS 86, 474
Matsuda T., Sekino N., Shima E., Sawada K., Spruit H. 1990, A&A 235, 211
Mon M. 1984, Thesis Université Paris VII
Peters G.J. 1972, PASP 84, 334
Poeckert R. 1981, PASP 93, 297
Poeckert R., Marlborough J.M. 1978, ApJS 38, 229
Suzuki M. 1980, PASJ 32, 331
Underhill A., Doazan V. 1982, Be stars with and without Emission Lines, Monograph series on nonthermal phenomena in stellar atmospheres (CNRS and NASA)